Research Article

Fangfang Yang, Yameng Song, Qin Wang, Yan Liu, and Aiqin Wang*

# Biomediated synthesis of ZnO quantum dots decorated attapulgite nanocomposites for improved antibacterial properties

https://doi.org/10.1515/gps-2022-0057
received February 14, 2022; accepted April 06, 2022

**Abstract:** Attapulgite (APT) is a natural one-dimensional clay mineral with good biocompatibility and has emerged as a promising nanomaterial for the construction of performance-enhanced nanocomposites. In this study, we developed a ZnO quantum dots-incorporated APT antibacterial nanocomposite by the *Aloe vera* extract-mediated green route. With the combined assistance of binding interactions of ZnO nuclei with APT and capping effect of active compounds in *Aloe vera* extract, the quantum-sized ZnO nanoparticles with hexagonal Wurtzite structure and sizes of <5 nm were uniformly decorated on the APT surface, resulting in a high-active antibacterial nanocomposite. The obtained ZnO/APT nanocomposites displayed favorable antibacterial activities, and the minimum inhibitory concentrations of the nanocomposite with ZnO loading of 20% against *E. coli* and *S. aureus* were 2.5 and 0.5 mg·mL$^{-1}$, respectively. This antibacterial performance was far better than that of APT and could almost be comparable to that of pure ZnO. For the green process, the phenolic compounds, proteins, and amino acids in *Aloe vera* extract were involved in the reduction and capping of ZnO, which contributed to a facile green strategy for preparation of the ZnO-modified APT nanocomposites. The present work provides new insight into the potential applications of APT in the antibacterial fields.

**Keywords:** ZnO, attapulgite, nanocomposite, phyto-mediated synthesis, antibacterial

## 1 Introduction

The development of antibiotic resistance has aggravated the difficulty in dealing with bacterial infections [1]. For decades, many efforts have been devoted to exploiting new antimicrobials to combat a variety of pathogenic microorganisms including resistant strains, which should be safe and efficient and induce little or no drug resistance. Currently, nanomaterials have received much attention in antibacterial applications [2], such as metal and metal oxide nanoparticles (NPs) [3] and carbon NPs [4]. The nanometer size effect, large surface area and adjustable shape give these nanomaterials unique antibacterial mechanisms, mainly including three viewpoints: reactive oxygen species (ROS) generation, release of antimicrobial ions, and direct interaction of NPs with bacteria inducing physical/mechanical damage [5–7]. Such multipathway bactericidal modes of action can avoid the occurrence of drug resistance, thus having more opportunities in the development of efficient and safe antimicrobials.

Nanoclay minerals, as naturally available nanomaterials, are widely concerned and used in the development of drug products for a long-standing time [8]. Due to the outstanding advantages of good biocompatibility, easy operability, and low-cost, nanoclay minerals have more potential values in the development of novel antibacterial materials [9,10]. Attapulgite (APT), one of the most abundant nanoclay minerals, is widely used in many fields in view of its special rod-like morphology, porous structure, large specific surface area, and high adsorption capacity [11]. More importantly, APT has inhibitory activities against bacteria based on the actions of the bacteria-adsorbed capability and physical-damage to

* **Corresponding author: Aiqin Wang,** Key Laboratory of Clay Mineral Applied Research of Gansu Province, Lanzhou Institute of Chemical Physics, Chinese Academy of Sciences, Lanzhou 730000, China, e-mail: aqwang@licp.cas.cn, tel: +86 931 4968118; fax: +86 931 4968019
**Fangfang Yang, Qin Wang:** Key Laboratory of Clay Mineral Applied Research of Gansu Province, Lanzhou Institute of Chemical Physics, Chinese Academy of Sciences, Lanzhou 730000, China
**Yameng Song, Yan Liu:** Key Laboratory of Clay Mineral Applied Research of Gansu Province, Lanzhou Institute of Chemical Physics, Chinese Academy of Sciences, Lanzhou 730000, China; Key Laboratory of Eco-Environment-Related Polymer Materials of Ministry of Education, Key Laboratory of Polymer Materials of Gansu Province, College of Chemistry and Chemical Engineering, Northwest Normal University, Lanzhou, 730070, China

the cell membrane of bacteria by its "elongate needle" shape [12]. Although the antimicrobial activity is not strong enough to be used as an antibacterial agent alone, APT has the advantages of acting as building blocks to combine with other antibacterial materials which would produce synergistic effects, obtaining more effective antibacterial properties [13,14]. For instance, the highly active surface of APT makes it favorable to be loaded with metal or metal oxide NPs [15], obtaining improved antibacterial properties by sustainably releasing active factors [16] and uniformly distributing NPs [17].

ZnO NPs are considered a promising antibacterial agent and have been used in feed additives, wound dressing, food preservation, and corrosion prevention owing to their broad-spectrum antibacterial activity, low-cost, and good thermal stability [18,19]. Incorporating ZnO NPs onto APT has been demonstrated to be an effective approach to strengthen the antibacterial performance of APT by synergistic effects. For example, Huo and Yang [20] prepared a ZnO/APT nanocomposite with enhanced antibacterial properties, in which ZnO NPs with a mean size of 15 nm were uniformly decorated on the APT surface. Many studies demonstrated that the antibacterial activity of ZnO NPs increased with the decrease in particle size [21–23]. Small-sized particles more easily bind to bacterial cells; more intimate contact of bacteria with ZnO NPs will produce stronger damage to cell membrane and wall of bacteria. Raghupathi et al. [24] compared the antibacterial activities of seven ZnO NPs with varying sizes and results showed that small-sized ZnO NPs could produce more disruption to bacterial cell wall, thus having higher antibacterial activity. In fact, except for the antibacterial action results from ROS generation via photocatalytic function, the main actions of ZnO depend on the NPs attachment to bacterial cells, which produce disruption or damage of cell membranes and release $Zn^{2+}$ [25]. Moreover, the concentration of oxygen vacancies on ZnO surface could be increased by reducing size [26], and more oxygen defect sites will generate more oxygen radicals or hydrogen peroxide inducing bacterial toxicity [27,28]. However, a concomitant problem with reducing the size of NPs is that the small NPs more easily agglomerate into larger particles, which has been highly concerned for the antibacterial activities of NPs. The agglomeration tendency increases the difficulties not only in the preparation of ZnO NPs with reduced size but also in the maintenance of stable properties. Previous studies have shown that plant-mediated synthesis process could control the particle size and morphology by capping the formed NPs to prevent them from agglomerating [29–32]. Moreover, currently, the method using natural plant extract for the preparation of metallic nanomaterials has also become the focus in NPs synthesis due to consideration of the green manufacture and safety requirements in health-related applications [33–35]. In addition to the advantages of greenness, mild reaction conditions, and convenient operations, another benefit of the green route involves the alleviation of biological toxicity and improvement of bioactivities [36–38]. Having said all of above, in order to obtain small-sized ZnO NPs on the APT surface, the phyto-mediated green strategy would be used to fabricate ZnO/APT nanocomposites. Due to the synergistic effects of phyto-mediated process and nucleation sites provided by APT, a smaller size and dispersion mode of ZnO NPs will be available, and ultimately obtain a ZnO/APT nanocomposite with favorable antibacterial properties.

Herein the ZnO quantum dots (QDs) decorated APT nanocomposites (ZnO/APT) were successfully developed via a phyto-mediated green route by using *Aloe vera* extract (ALE) as a reduction and stabilizing agent. Owing to the enhanced antibacterial activities of reduced size of ZnO NPs, the ZnO QDs-incorporated APT possesses favorable antibacterial efficacy against both gram-negative and gram-positive bacteria. In this work, ZnO QDs exerted main roles for the antibacterial enhancement of APT, as well APT served as a structural platform to facilitate ZnO QDs dispersion, thus a synergistic effect was produced to maximize the antibacterial ability of the nanocomposite. In addition, the mild and simple green procedure avoids potential toxicity to the environment and organisms and provides a more green and safe antibacterial nanomaterial, which makes the nanocomposites to be applied in wider antibacterial fields.

# 2 Materials and methods

## 2.1 Materials

*Aloe vera* was obtained from the local market, Gansu, China. APT mineral powder was provided by Xuyi Oubaite Clay Materials Co., Ltd (Jiangsu, China), and the main compositions consisted of CaO (0.49%), $Al_2O_3$ (10.73%), MgO (9.70%), $SiO_2$ (60.83%), $K_2O$ (1.18%), and $Fe_2O_3$ (5.71%), as determined by X-ray fluorescence. Zinc nitrate hexahydrate ($Zn(NO_3)_2{\cdot}6H_2O$, ≥99%) was purchased from Xilong Scientific Co., Ltd (Guangzhou, China). Sodium hydroxide (NaOH, ≥96%) was purchased from Tianjin Kermel Chemical Reagent Co., Ltd (Tianjin, China). Nutrient agar medium and LB broth medium were purchased from Qingdao Hope Bio-Technology Co., Ltd, China.

## 2.2 Preparation of ALE

Fresh leaves of *Aloe vera* were cleaned thoroughly using distilled water to remove all dust particles and dried in shade to remove all the moisture on the surface before being chopped into pieces. Twenty grams of chopped *Aloe vera* was mixed with 100 mL of distilled water and heated to 60°C in a water bath for 30 min. The mixture was cooled to room temperature and filtered using Whatman No.1 filter paper to obtain ALE.

## 2.3 Green synthesis of ZnO and ZnO/APT nanocomposites

ZnO/APT nanocomposites with different theoretical loads of ZnO were prepared using the following procedure. APT (3 g) was added to 30 mL of ALE diluted with 20 mL of distilled water, and stirred continually for 10 min at 300 rpm. An aqueous solution of $Zn(NO_3)_2{\cdot}6H_2O$ prepared by dissolving 0.55, 1.1, 2.2, 3.3, and 4.4 g (corresponding to the theoretical ZnO loadings of 5%, 10%, 20%, 30%, and 40%) $Zn(NO_3)_2{\cdot}6H_2O$ in 50 mL of distilled water was then added to the above suspension by dripping slowly under stirring at 600 rpm. The mixture (pH 8) was stirred for 60 min at 80°C under reflux cooling. Finally, the white precipitate was collected by centrifugation at 12,000 rpm, washed 2 times with distilled water and 1 time with ethanol, and then dried for 24 h at 80°C in an air oven. ZnO NPs were prepared similar to the preparation method of ZnO/APT nanocomposites, namely, 2.97 g $Zn(NO_3)_2{\cdot}6H_2O$ in 50 mL of distilled water was slowly dropped to 30 mL of ALE diluted by 20 mL of distilled water under stirring at 600 rpm. The next procedure is the same as above.

## 2.4 Characterization

High-resolution transmission electron microscope images (HRTEM) and selective area electron diffraction pattern (SAED) were characterized using JEM-2100 (JEOL, Japan) and Tecnai G2 F20 S-TWIN (158 Hillsboro, OR, USA) microscopes. X-ray diffraction (XRD) patterns were obtained from an X'Pert PRO diffractometer (PAN analytical Co., Netherlands) equipped with Cu-Kα radiation sources of 40 mA and 40 kV. Fourier transform infrared (FTIR) spectra were obtained on Nicolet Is50 FTIR spectrophotometer (Thermo Scientific, USA) in the range of 4,000–400 $cm^{-1}$ using KBr pellets. UV-visible (UV-Vis) spectra were recorded by a UV-1900i spectrometer (Shimadzu, Japan). The particle size distribution of the samples is determined by a Malvern Zetasizer Nano system (ZEN3600, Malvern, UK) companying a 633 nm He–Ne laser irradiation.

## 2.5 Antibacterial activity assay

The antibacterial activities of the samples were evaluated by the minimum inhibitory concentration (MIC) values using the agar plate dilution method and the inhibition zone diameters tested using disk diffusion method. The strains of *Staphylococci aureus* (*S. aureus*, ATCC 25923) and *Escherichia coli* (*E. coli*, ATCC 25922) from clinical isolates were provided by the Laboratory Medicine Center, Lanzhou University Second Hospital, China. Briefly, all samples were sterilized under a UV lamp for 2 h. For the MIC values test, the different amounts of antibacterial materials were well mixed with 20 mL of agar mediums to obtain the mixtures with concentrations of 0.1, 0.25, 0.5, 1.0, 2.5, 5.0, 10.0 $mg{\cdot}mL^{-1}$, and then the mixtures were poured into the plates and obtained the sample plates. After that 1–2 µL of $10^4$ $CFU{\cdot}mL^{-1}$ fresh bacterial liquid was seeded on the medium at 3 different positions. Finally, the inoculated plates were incubated at 37°C for 24 h. The MIC values were determined according to the lowest concentrations to inhibit the growth of all strains thoroughly. Positive control groups with the absence of sample and negative control groups without both sample and bacterial strain were included in this work. For the inhibition zone diameters test, the ager plates with bacterial concentration of $10^5$ $CFU{\cdot}mL^{-1}$ were prepared, and the discs of diameter of 10 mm were impregnated with 30 mL of the sample solutions that had a concentration of 0.5 $g{\cdot}mL^{-1}$ and then placed on the inoculated plates. The plates were incubated at 37°C for 24 h and after incubation, the inhibition zone diameter values (mm) around the discs were measured using a vernier caliper. All tests were performed in triplicate.

# 3 Results and discussion

## 3.1 Formation and characterization of ZnO/APT nanocomposites

In this study, the nanocomposites of ZnO QDs loaded APT were prepared by the ALE-mediated one-pot process (Scheme 1). The formation of ZnO/APT nanocomposites was confirmed by structural characterizations using UV-Vis spectroscopy, HRTEM, XRD, and FTIR.

## 3.2 UV-Vis spectroscopic analysis

The UV-Vis absorption spectroscopy for ZnO and ZnO/APT under different reaction times was analyzed to investigate the formation and properties of ZnO/APT nanocomposites. The UV-Vis spectra of all samples were recorded after diluted for 5-multiply of the original suspension. The results of UV-Vis analysis are shown in Figure 1. From the spectroscopy of pure ZnO as shown in Figure 1a, it is displayed that a strong and sharper absorption band at 365 nm is presented suffering a reaction time of 1 h, indicating that relatively homogeneous ZnO particles were formed in the aqueous suspension. However, with the time increasing to 1.5 h, some particles agglomerated and formed larger ZnO particles, which can be confirmed from the particle size distribution of pure ZnO from dynamic light scattering analysis (Figure A1 in Appendix). The same result was also manifested in Figure 1b that displayed the spectroscopy of ZnO/APT, in which the ZnO QDs can be formed after 1 h reaction time. What is noteworthy is that the characteristic absorption band for ZnO/APT occurred at 357 nm had a shortwave shift compared to that of pure ZnO particles (Figure 1c), which was possibly caused by the particle size decrease of ZnO and quantum confinement effect [39,40]. Figure 1d shows the spectroscopy of ZnO/APT nanocomposites with different theoretical loading amounts of ZnO. It is found that the absorption bands become sharper with increase in the loadings of ZnO, which can be attributed to the increase in the concentrations of ZnO NPs in the aqueous suspensions. In fact, as shown in Table 1, the actual yields of ZnO in ZnO/APT nanocomposites that were confirmed by X-ray fluorescence were not consistent with the theoretical values that determined the amount of zinc salt added. When the loading amounts of ZnO were 5%, 10%, and 20%, the actual yields of ZnO were near the theoretical values, while the actual yields of ZnO were below the theoretical yields when the loading of ZnO was set to 30% and 40%. These results were consistent with the subsequent results of antibacterial performance of ZnO/APT nanocomposites, where the antibacterial activities showed no remarkable increase with the increase in the loadings of ZnO from 20% to 40%.

## 3.3 Structural and morphological analysis of pure ZnO, APT, and ZnO/APT nanocomposite by HRTEM and XRD

The microscopic morphology of ZnO/APT nanocomposite was analyzed by HRTEM. Here considering the fact that the best antibacterial performance occurred in the nanocomposite containing 20% ZnO, ZnO/APT-20% as the optimum combination was explored in more detail to confirm the successful production of the quantum-sized


**Scheme 1:** Schematic illustration of the preparation process for ZnO/APT nanocomposites.

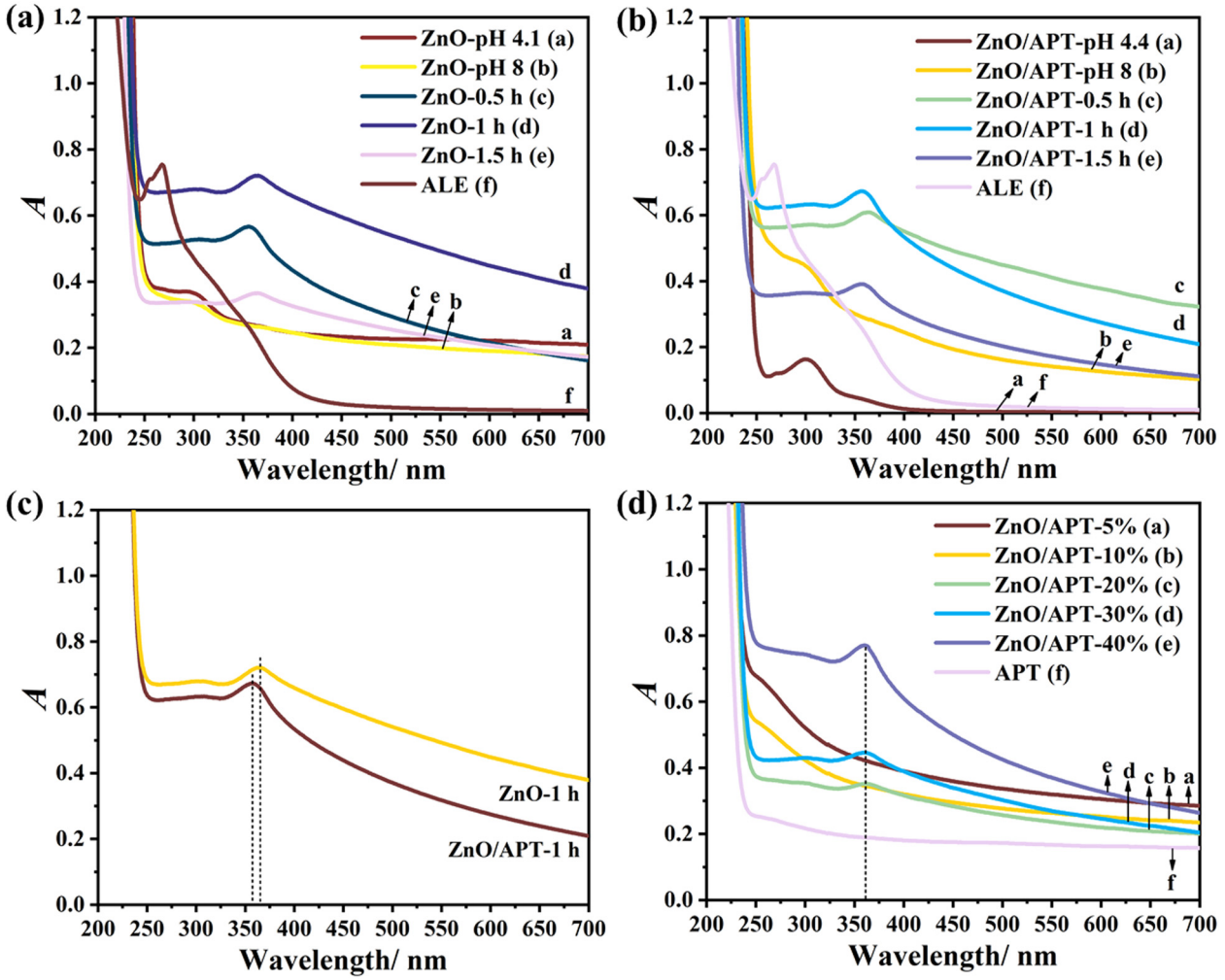


**Figure 1:** UV-Vis spectra of ALE, APT, ZnO, and ZnO/APT nanocomposites: (a) ZnO and (b) ZnO/APT-20% with different reaction times, (c) ZnO and (b) ZnO/APT-20% after 1 h of reaction, and (d) APT and ZnO/APT nanocomposites with ZnO loadings of 5, 10, 20, 30, and 40%.

**Table 1:** The actual ZnO loading amounts in ZnO/APT nanocomposites as determined by X-ray fluorescence

| Samples | The percentages of ZnO content (%) |
|---|---|
| ZnO/APT-5% | 5.70 |
| ZnO/APT-10% | 10.53 |
| ZnO/APT-20% | 19.19 |
| ZnO/APT-30% | 24.99 |
| ZnO/APT-40% | 32.53 |

ZnO nanoparticles on the APT surface. Moreover, the microscopic morphologies of pure ZnO and APT were also observed for comparison. Figure 2 shows the HRTEM images of ZnO and APT. It is found that the spherical polycrystalline ZnO nanostructures with dimensions of approximately 200 nm were formed in the green process (Figure 2a–c), and the APTs exhibited rod-like morphology and their surfaces were clean and had no fixtures (Figure 2d–f). Notably, the ZnO particles have a comparatively looser structure, which may be relevant with the attachment of phytochemical from ALE. In contrast, ZnO NPs were present on the surface of the APT nanorods that were observed in the microscopic images of ZnO/APT-20% shown in Figure 3. It can be confirmed from Figure 3c–e that the particle sizes of crystalline ZnO formed on the APT surface were below 5 nm which can be defined as ZnO QDs, suggesting that the APT nanorods had good dispersion effect to ZnO NPs. Attributed to the presence of Si-OH groups on APT surface, it can be speculated which could bind with the crystal nuclei of ZnO by H-bonding interactions, followed by the seed growth of ZnO to form ZnO QDs on the APT surface. Meanwhile, the crystal growth of ZnO was inhibited by capping of active molecules from ALE. Therefore, the combining influential effect of APT and the phyto-mediated process played a decisive role in the formation of quantum-sized ZnO NPs. The SAED pattern in

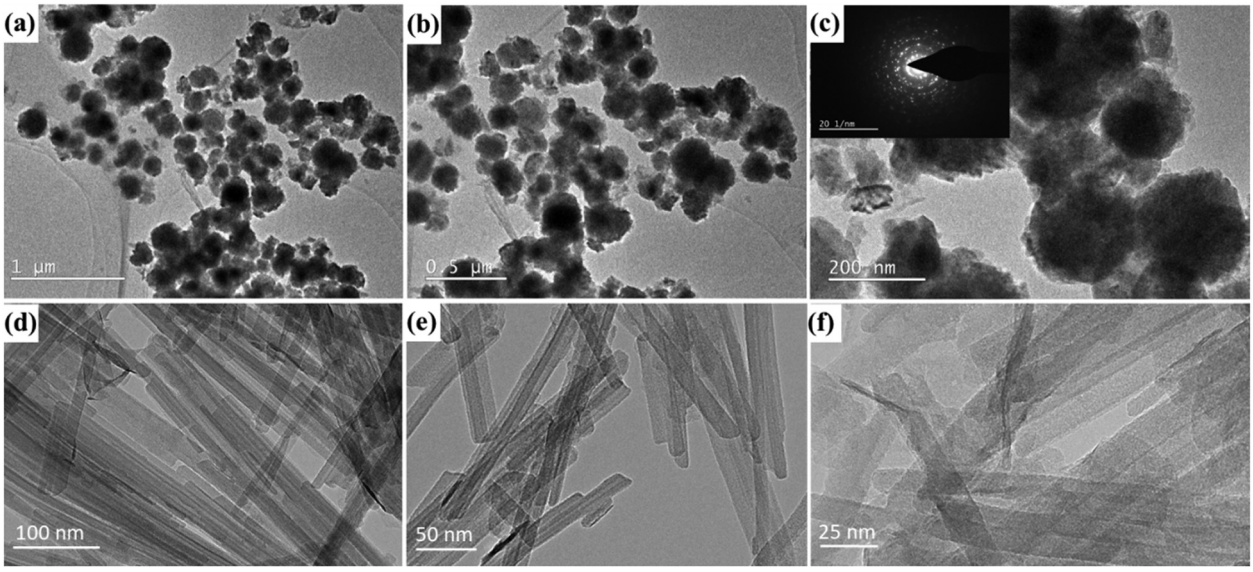


**Figure 2:** HRTEM images of ZnO (a–c) and APT (d–f). The insert in (c) is selected electron diffraction pattern of ZnO nanostructure.

Figure 3f indicates the formation of polycrystalline ZnO NPs on the APT surface. In addition, the formation of crystalline ZnO was further confirmed by XRD analysis. As shown in Figure 4, the characteristic diffraction peaks corresponding to the pure hexagonal Wurtzite structure of ZnO appeared in both pure ZnO and ZnO/APT nanocomposites with loading amounts of 20%, 30%, and 40%, suggesting the successful formation of ZnO during the green synthesis process. The strong and sharp diffraction peaks manifested that the phyto-mediated ZnO has a good crystalline structure. Moreover, no indication of a secondary phase and other impure peaks were observed in the patterns of ZnO and ZnO/APT, indicating that no impurity phase such as $Zn(OH)_2$ was formed in ZnO and ZnO/APT nanocomposites. For ZnO/APT-5% and ZnO/APT-10%, there were no obvious diffraction peaks of ZnO, which may be caused by the fact that the content of ZnO was too low and below the detection limit of XRD. In conclusion, based on the binding interactions of APT and the capping effect of active molecules, small-sized ZnO NPs were formed

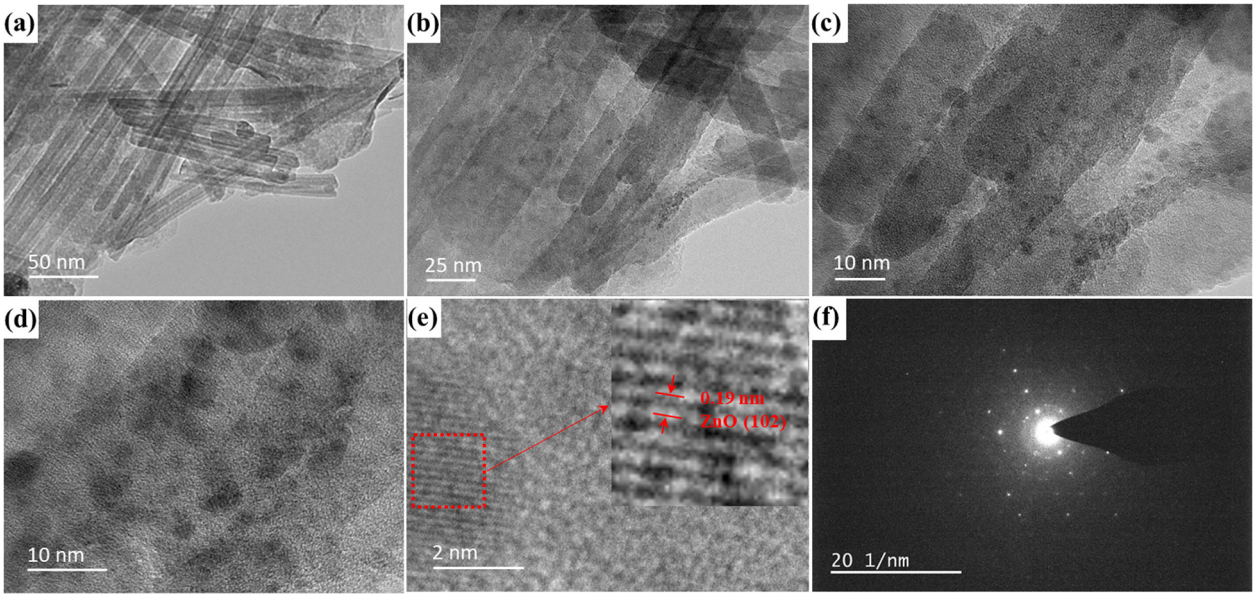


**Figure 3:** (a–e) HRTEM images and (f) the corresponding selected electron diffraction pattern of ZnO/APT-20% nanocomposite.

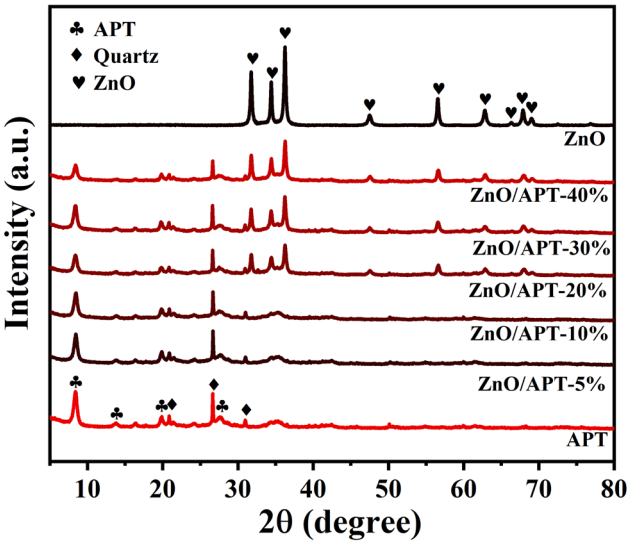


**Figure 4:** XRD pattern of pure ZnO, APT, and ZnO/APT nanocomposites with ZnO loadings of 5%, 10%, 20%, 30%, and 40%.

on the surface of APT nanorods, which was responsible for the improvement in the antibacterial performance of APT.

## 3.4 FTIR analysis of ALE, pure ZnO, APT, and ZnO/APT nanocomposites

Furthermore, the special interactions between ZnO QDs and APT and the biomolecules responsible for the reduction and capping of ZnO were investigated by FTIR spectrum as demonstrated in Figure 5. In the spectrum of ALE (Figure 5a), the band at 3,100–3,800 $cm^{-1}$ can be attributed

**Table 2:** MIC values of APT, pure ZnO, and ZnO/APT nanocomposites

| Samples | Antibacterial activity (MIC in mg·$mL^{-1}$) | |
|---|---|---|
| | *E. coli* | *S. aureus* |
| APT | >10 | >5 |
| ZnO | 2.5 | 0.25 |
| ZnO/APT-5% | 5 | 1 |
| ZnO/APT-10% | 5 | 1 |
| ZnO/APT-20% | 2.5 | 0.5 |
| ZnO/APT-30% | 2.5 | 0.5 |
| ZnO/APT-40% | 2.5 | 0.5 |

to the characteristic stretching vibrations of the –OH group from phenol and the vibrations of the $-NH_2$ group of amines [41]. The band at 2,940 and 1,726 $cm^{-1}$ are respectively assigned to the –CH stretching of alkanes and the stretching vibrations of the –C═O group in ketones, aldehydes, and carboxylic acids [42], and the 1,591 $cm^{-1}$ band may be due to the amine groups from proteins and enzymes. The bands at the range of 1,500–400 $cm^{-1}$ are involved in the C–H deformation vibration, C–C stretching and skeleton vibration, and N–H angular deformation [43]. For pure ZnO derived from ALE (Figure 5a), the vibration band of 466 $cm^{-1}$ corresponded to Zn–O stretching vibration clearly showing the formation of crystalline ZnO [44], and the other bands appeared in the range 500–4,000 $cm^{-1}$ representing the vibration of biomolecules attached to the ZnO particles surface [45]. The bands at 885 and 699 $cm^{-1}$ attribute to C–H vibrations of alkanes and aromatic rings, respectively [46,47]. The band at 1,030 $cm^{-1}$ corresponds to C–N stretching vibration of amine [48], and the peak at 1,085 $cm^{-1}$ can be

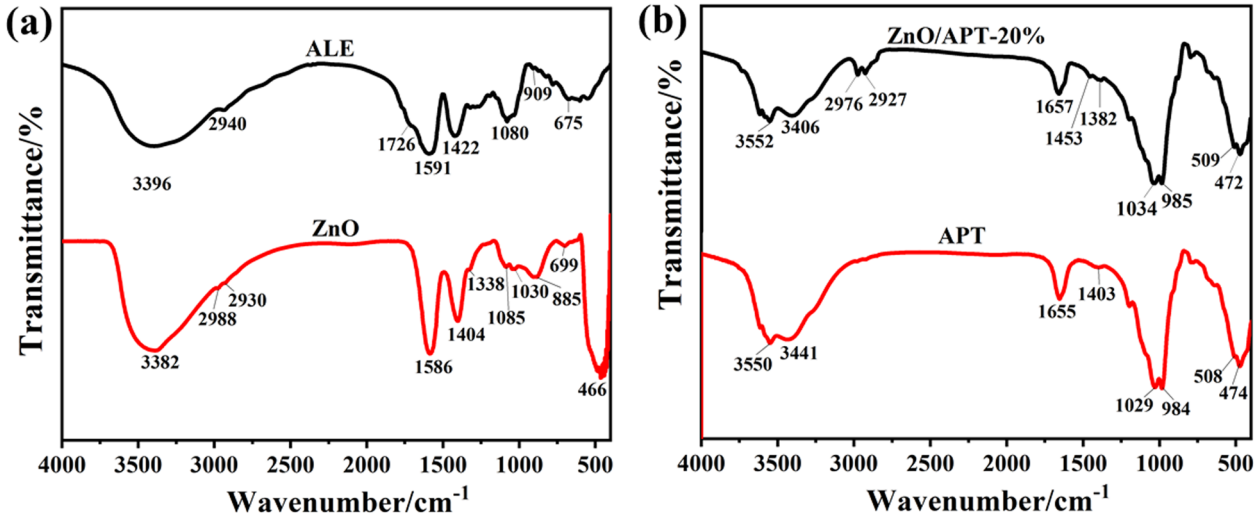


**Figure 5:** FTIR patterns of (a) ALE and pure ZnO and (b) APT and ZnO/APT-20% nanocomposite.

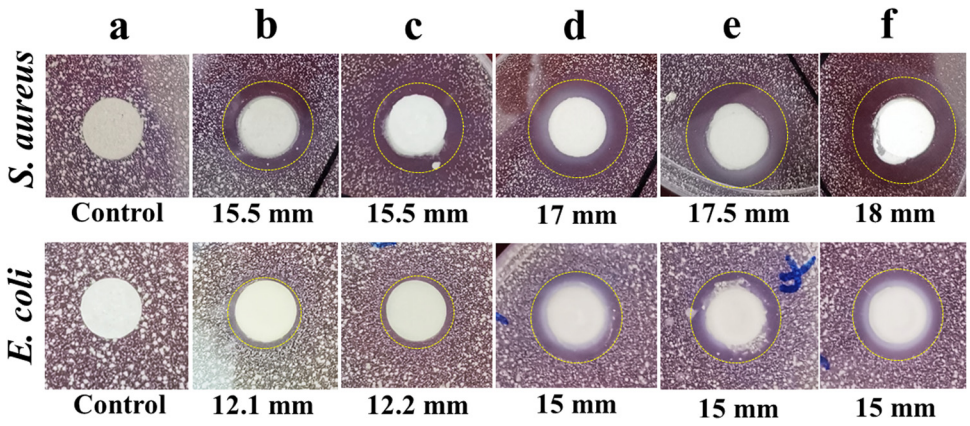


**Figure 6:** The inhibition zone diameters of ZnO/APT nanocomposites with different loading amounts of ZnO. The alphanumeric numbers of a–f refer to control groups, ZnO/APT-5%, ZnO/APT-10%, ZnO/APT-20%, ZnO/APT-30%, and ZnO/APT-40%, respectively.

attributed to C–O stretching from the polyphenolic compound in ALE [49,50]. The signals at 1,338 and 1,404 $cm^{-1}$ bands correspond to O–H bending from hydroxyl/phenol groups and the symmetric stretching of the carboxyl side groups in the amino acid residues of the protein [51,52]. In addition, the appearance of 1,586 $cm^{-1}$ band is due to C–N stretching vibration of protein amide linkages. It is concluded that the presence of the hydroxyl groups, amine groups, and aromatic groups from phenols and proteins suggested the adsorption of biomolecules on ZnO particles, which were responsible for the reduction and stabilization of crystalline ZnO. In addition, it is found from Figure 5b that the band shifts occurred at 3,392, 1,653, and 1,433 $cm^{-1}$ in the FTIR spectrum of ZnO/APT compared to that of APT, which confirms the formation of ZnO NPs on APT by the H-bonding interactions with the surface silanol groups of APT.

### 3.5 Antibacterial activities of ZnO/APT nanocomposites

The above structural characterizations of ZnO/APT nanocomposites fully confirmed the successful formation of ZnO QDs on the APT surface, which would contribute to the enhanced antibacterial properties of APT. In this study, the antibacterial activities of ZnO, APT, and ZnO/APT nanocomposites with different ZnO loadings against *E. coli* and *S. aureus* were evaluated by testing MIC values (Table 2, Figures A2 and A3). Moreover, the inhibition zone diameters of ZnO/APT nanocomposites were tested to further analyze the antibacterial performance of the nanocomposites with increase in the ZnO content (Figure 6). It is shown that APT had no inhibition activities with concentrations below 5 $mg{\cdot}mL^{-1}$. The synthesized ZnO particles exhibited considerable inhibition activities with MIC values up to 2.5 and 0.25 $mg{\cdot}mL^{-1}$ against *E. coli* and *S. aureus*, respectively. For the ZnO/APT nanocomposites, with ZnO loadings increasing from 5% to 20%, the antibacterial activities increased, while the MIC values no longer increased with ZnO loadings further increasing from 20% to 40%. The MIC values of ZnO/APT-20% against *E. coli* and *S. aureus* were 2.5 and 0.5 $mg{\cdot}mL^{-1}$, respectively. Furthermore, it can be found from Figure 6 that the inhibition zone diameters toward *S. aureus* increased from 15.5 to 17 mm with ZnO loadings added from 5% to 20%, and then showed a slight increase from 20% to 40%. The change trend against *E. coli* was completely consistent with the MIC values, and the inhibition zone diameter of ZnO/APT-20% was 15 mm. The *S. aureus*, in general, was more sensitive to the green-prepared ZnO/APT nanocomposites that *E. coli*. These results indicated that the incorporation of ZnO QDs significantly improved the antibacterial performance of APT, which is attributed to the anchoring and dispersion of ZnO NPs provided by APT as well as the capping reaction of biomolecules in ALE.

## 4 Conclusion

In the present study, the ZnO QDs-incorporated APT antibacterial nanocomposites were successfully prepared through the phyto-mediated green strategy, in which the phytochemical from *Aloe vera* were only used as reducing and capping agents. Due to the interfacial interactions of APT with the ZnO nuclei combined with the capping effects contributed from the biomolecules of ALE, small-sized ZnO NPs with diameters below 5 nm were decorated on the surface of APT nanorods, which is responsible for the improved

antibacterial activities of the nanocomposites. The antibacterial results gave information that the inhibition activities of ZnO/APT nanocomposites increased with the increase in the ZnO loadings from 5% to 20%, and ZnO/APT-20% exhibited favorable antibacterial activities with the MIC values of 2.5 and 0.5 $mg{\cdot}mL^{-1}$ against *E. coli* and *S. aureus*, respectively, which can be attributed to the decrease in the actual ZnO yields and possible increase in the size of ZnO NPs. The favorable antibacterial performance and the eco-friendly process recommend the developed ZnO/APT nanocomposites as a promising candidate in antibacterial applications.

**Funding information:** The research was funded by the Foundation for the Major Projects of the Regional Key Project of the Science and Technology Service of the Chinese Academy of Sciences, China (KFJ–STS–QYZX–086), the Special Fund Project of High Technology Development of Gansu Province (no. 2021000105), the Youth Cooperation Fund of Lanzhou Institute of Chemical Physics, China (HZJJ20–08), and the Natural Science Foundation of Gansu, China (21JR7RA079).

**Author contributions:** Fangfang Yang: investigation and writing – original draft; Yameng Song: investigation and software; Qin Wang: methodology and data curation; Yan Liu: validation and formal analysis; Aiqin Wang: resources, conceptualization, methodology, and writing – review and editing.

**Conflict of interest:** Authors state no conflict of interest.

**Data availability statement:** The data used to support the findings of this study are available from the corresponding author upon request.

# References

[1] Rather IA, Kim BC, Bajpai VK, Park YH. Self-medication and antibiotic resistance: Crisis, current challenges, and prevention. Saudi J Biol Sci. 2017;24(4):808–12. doi: 10.1016/j.sjbs.2017.01.004.

[2] Wang Y, Yang Y, Shi Y, Song H, Yu C. Antibiotic-free antibacterial strategies enabled by nanomaterials: Progress and perspectives. Adv Mater. 2020;32(18):e1904106. doi: 10.1002/adma.201904106.

[3] Gold K, Slay B, Knackstedt M, Gaharwar AK. Antimicrobial activity of metal and metal-oxide based nanoparticles. Adv Ther. 2018;1(3):1700033. doi: 10.1002/adtp.201700033.

[4] Maleki Dizaj S, Mennati A, Jafari S, Khezri K, Adibkia K. Antimicrobial activity of carbon-based nanoparticles. Adv Pharm Bull. 2015;5(1):19–23. doi: 10.5681/apb.2015.003.

[5] Al-Jumaili A, Alancherry S, Bazaka K, Jacob MV. Review on the antimicrobial properties of carbon nanostructures. Materials. 2017;10(9):1066. doi: 10.3390/ma10091066.

[6] Pulingam T, Thong KL, Ali ME, Appaturi JN, Dinshaw IJ, Ong ZY, et al. Graphene oxide exhibits differential mechanistic action towards Gram-positive and Gram-negative bacteria. Colloid Surf B. 2019;181:6–15. doi: 10.1016/j.colsurfb.2019.05.023.

[7] Slavin YN, Asnis J, Hafeli UO, Bach H. Metal nanoparticles: understanding the mechanisms behind antibacterial activity. J Nanobiotechnol. 2017;15(1):65. doi: 10.1186/s12951-017-0308-z.

[8] Saadat S, Pandey G, Tharmavaram M, Braganza V, Rawtani D. Nano-interfacial decoration of halloysite nanotubes for the development of antimicrobial nanocomposites. Adv Colloid Interface Sci. 2020;275:102063. doi: 10.1016/j.cis.2019.102063.

[9] Ruiz-Hitzky E, Darder M, Fernandes FM, Wicklein B, Alcântara ACS, Aranda P. Fibrous clays based bionanocomposites. Prog Polym Sci. 2013;38(10–11):1392–414. doi: 10.1016/j.progpolymsci.2013.05.004.

[10] Wang CY, Makvandi P, Zare EN, Tay FR, Niu LN. Advances in antimicrobial organic and inorganic nanocompounds in biomedicine. Adv Ther. 2020;3(8):2000024. doi: 10.1002/adtp.202000024.

[11] Zhang J, Jiang W, Jiang J, Wu M, Shi Y, Mao P, et al. One-pot synthesis of sulfonated carbon/palygorskite solid-acid catalyst for the esterification of oleic acid with methanol. Clays Clay Min. 2021;69:389–96. doi: 10.1007/s42860-021-00137-6.

[12] Cai X, Zhang J, Ouyang Y, Ma D, Tan S, Peng Y. Bacteria-adsorbed palygorskite stabilizes the quaternary phosphonium salt with specific-targeting capability, long-term antibacterial activity, and lower cytotoxicity. Langmuir. 2013;29(17):5279–85. doi: 10.1021/la400824f.

[13] Liu J, Gao Z, Liu H, Pang L, He X, Hui A, et al. A study on improving the antibacterial properties of palygorskite by using cobalt-doped zinc oxide nanoparticles. Appl Clay Sci. 2021;209:106112. doi: 10.1016/j.clay.2021.106112.

[14] Shu Z, Zhang Y, Yang Q, Yang H. Halloysite nanotubes supported Ag and ZnO nanoparticles with synergistically enhanced antibacterial activity. Nanoscale Res Lett. 2017;12(1):135. doi: 10.1186/s11671-017-1859-5.

[15] Aranda P, Ruiz-Hitzky E. Immobilization of nanoparticles on fibrous clay surfaces: Towards promising nanoplatforms for advanced functional applications. Chem Rec. 2018;18(7–8):1125–37. doi: 10.1002/tcr.201700113.

[16] Wang J, Liu Y, Liu B, Wu Y. Preparation and antibacterial effect of nanopalygorskite supported nano-silver powder. Adv Mater Res. 2014;1052:327–31. doi: 10.4028/www.scientific.net/AMR.1052.327.

[17] Wang W, Li Y, Wang W, Gao B, Wang Z. Palygorskite/silver nanoparticles incorporated polyamide thin film nanocomposite membranes with enhanced water permeating, antifouling and antimicrobial performance. Chemosphere. 2019;236:124396. doi: 10.1016/j.chemosphere.2019.124396.

[18] Jiang S, Lin K, Cai M. ZnO nanomaterials: current advancements in antibacterial mechanisms and applications. Front Chem. 2020;8:580. doi: 10.3389/fchem.2020.00580.

[19] Karaköse E, Çolak H, Duman F. Green synthesis and antimicrobial activity of ZnO nanostructures *Punica granatum* shell

extract. Green Process Synth. 2017;6(3):317–23. doi: 10.1515/gps-2016-0190.
[20] Huo C, Yang H. Synthesis and characterization of ZnO/palygorskite. Appl Clay Sci. 2010;50(3):362–6. doi: 10.1016/j.clay.2010.08.028.
[21] Talebian N, Amininezhad SM, Doudi M. Controllable synthesis of ZnO nanoparticles and their morphology-dependent antibacterial and optical properties. J Photoch Photobio B. 2013;120:66–73. doi: 10.1016/j.jphotobiol.2013.01.004.
[22] Abebe B, Zereffa EA, Tadesse A, Murthy HCA. A review on enhancing the antibacterial activity of ZnO: Mechanisms and microscopic investigation. Nanoscale Res Lett. 2020;15(1):190. doi: 10.1186/s11671-020-03418-6.
[23] Lallo da Silva B, Caetano BL, Chiari-Andreo BG, Pietro R, Chiavacci LA. Increased antibacterial activity of ZnO nanoparticles: Influence of size and surface modification. Colloid Surf B. 2019;177:440–7. doi: 10.1016/j.colsurfb.2019.02.013.
[24] Raghupathi KR, Koodali RT, Manna AC. Size-dependent bacterial growth inhibition and mechanism of antibacterial activity of zinc oxide nanoparticles. Langmuir. 2011;27(7):4020–8. doi: 10.1021/la104825u.
[25] Joe A, Park SH, Shim KD, Kim DJ, Jhee KH, Lee HW, et al. Antibacterial mechanism of ZnO nanoparticles under dark conditions. J Ind Eng Chem. 2017;45:430–9. doi: 10.1016/j.jiec.2016.10.013.
[26] Zhang Q, Xu M, You B, Zhang Q, Yuan H, Ostrikov K. Oxygen vacancy-mediated ZnO nanoparticle photocatalyst for degradation of methylene blue. Appl Sci. 2018;8(3):353. doi: 10.3390/app8030353.
[27] Hirota K, Sugimoto M, Kato M, Tsukagoshi K, Tanigawa T, Sugimoto H. Preparation of zinc oxide ceramics with a sustainable antibacterial activity under dark conditions. Ceram Int. 2010;36(2):497–506. doi: 10.1016/j.ceramint.2009.09.026.
[28] Xu X, Chen D, Yi Z, Jiang M, Wang L, Zhou Z, et al. Antimicrobial mechanism based on $H_2O_2$ generation at oxygen vacancies in ZnO crystals. Langmuir. 2013;29(18):5573–80. doi: 10.1021/la400378t.
[29] Md Ishak NAI, Kamarudin SK, Timmiati SN. Green synthesis of metal and metal oxide nanoparticles via plant extracts: An overview. Mater Res Express. 2019;6(11):112004. doi: 10.1088/2053-1591/ab4458.
[30] Yuvakkumar R, Suresh J, Nathanael AJ, Sundrarajan M, Hong SI. Novel green synthetic strategy to prepare ZnO nanocrystals using Rambutan (*Nephelium lappaceum* L.) peel extract and its antibacterial applications. Mater Sci Eng C. 2014;41:17–27. doi: 10.1016/j.msec.2014.04.025.
[31] Song JY, Jang H-K, Kim BS. Biological synthesis of gold nanoparticles using *Magnolia kobus* and *Diopyros kaki* leaf extracts. Proc Biochem. 2009;44(10):1133–8. doi: 10.1016/j.procbio.2009.06.005.
[32] Sri Sindhura K, Prasad TNVKV, Panner Selvam P, Hussain OM. Synthesis, characterization and evaluation of effect of phytogenic zinc nanoparticles on soil exo-enzymes. Appl Nanosci. 2013;4(7):819–27. doi: 10.1007/s13204-013-0263-4.
[33] Hernandez-Diaz JA, Garza-Garcia JJ, Zamudio-Ojeda A, Leon-Morales JM, Lopez-Velazquez JC, Garcia-Morales S. Plant-mediated synthesis of nanoparticles and their antimicrobial activity against phytopathogens. J Sci Food Agric. 2021;101(4):1270–87. doi: 10.1002/jsfa.10767.
[34] Singh A, Gautam PK, Verma A, Singh V, Shivapriya PM, Shivalkar S, et al. Green synthesis of metallic nanoparticles as effective alternatives to treat antibiotics resistant bacterial infections: A review. Biotechnol Rep. 2020;25:e00427. doi: 10.1016/j.btre.2020.e00427.
[35] Bawazeer S, Rauf A, Shah SUA, Shawky AM, Al-Awthan YS, Bahattab OS, et al. Green synthesis of silver nanoparticles using *Tropaeolum majus*: Phytochemical screening and antibacterial studies. Green Process Synth. 2021;10(1):85–94. doi: 10.1515/gps-2021-0003.
[36] Gunalan S, Sivaraj R, Rajendran V. Green synthesized ZnO nanoparticles against bacterial and fungal pathogens. Prog Nat Sci Mater. 2012;22(6):693–700. doi: 10.1016/j.pnsc.2012.11.015.
[37] Sathishkumar M, Pavagadhi S, Mahadevan A, Balasubramanian R. Biosynthesis of gold nanoparticles and related cytotoxicity evaluation using A549 cells. Ecotoxicol Env Saf. 2015;114:232–40. doi: 10.1016/j.ecoenv.2014.03.020.
[38] Ashraf N, Sumrra SH, Assiri MA, Usman M, Hussain R, Aziz F, et al. Digera muricata (L.) Mart. mediated synthesis of antimicrobial and enzymatic inhibitory zinc oxide bionanoparticles. Green Process Synth. 2021;10(1):476–84. doi: 10.1515/gps-2021-0044.
[39] Kumar H, Rani R. Structural and optical characterization of ZnO nanoparticles synthesized by microemulsion route. ILC Phys Astron. 2013;14:26–36.
[40] Zandi S, Kameli P, Salamati H, Ahmadvand H, Hakimi M. Microstructure and optical properties of ZnO nanoparticles prepared by a simple method. Phys B. 2011;406(17):3215–8. doi: 10.1016/j.physb.2011.05.026.
[41] Ali K, Dwivedi S, Azam A, Saquib Q, Al-Said MS, Alkhedhairy AA, et al. *Aloe vera* extract functionalized zinc oxide nanoparticles as nanoantibiotics against multi-drug resistant clinical bacterial isolates. J Colloid Interface Sci. 2016;472:145–56. doi: 10.1016/j.jcis.2016.03.021.
[42] Chandran SP, Chaudhary M, Pasricha R, Ahmad A, Sastry M. Synthesis of gold nanotriangles and silver nanoparticles using *Aloe vera* plant extract. Biotechnol Prog. 2006;22(2):577–83. doi: 10.1021/bp0501423.
[43] Chaudhary A, Kumar N, Kumar R, Salar RK. Antimicrobial activity of zinc oxide nanoparticles synthesized from *Aloe vera* peel extract. SN Appl Sci. 2018;1(1):136. doi: 10.1007/s42452-018-0144-2.
[44] Samavati Z, Samavati A, Ismail AF, Yahya N, Othman MHD, Rahman MA, et al. The impact of ZnO configuration as an external layer on the sensitivity of a bi-layer coated polymer optical fiber probe. RSC Adv. 2020;10(22):12864–75. doi: 10.1039/D0RA00243G.
[45] Gutha Y, Pathak JL, Zhang W, Zhang Y, Jiao X. Antibacterial and wound healing properties of chitosan/poly(vinyl alcohol)/zinc oxide beads (CS/PVA/ZnO). Int J Biol Macromol. 2017;103:234–41. doi: 10.1016/j.ijbiomac.2017.05.020.
[46] Jose LM, Raj RSA, Sajan D, Aravind A. Adsorption and photocatalytic activity of biosynthesised ZnO nanoparticles using *Aloe vera* leaf extract. Nano Exp. 2021;2(1):010039. doi: 10.1088/2632-959X/abeec6.
[47] Archana B, Manjunath K, Nagaraju G, Chandra Sekhar KB, Kottam N. Enhanced photocatalytic hydrogen generation and photostability of ZnO nanoparticles obtained via green

synthesis. Int J Hydrog Energ. 2017;42(8):5125–31. doi: 10.1016/j.ijhydene.2016.11.099.
[48] Bhuiyan MNI, Begum J, Sultana M. Chemical composition of leaf and seed essential oil of *Coriandrum sativum* L. from Bangladesh. Bangl J Pharmacol. 2009;4(2):150–3. doi: 10.3329/bjp.v4i2.2800.
[49] Sabaa MW, Abdallah HM, Mohamed NA, Mohamed RR. Synthesis, characterization and application of biodegradable crosslinked carboxymethyl chitosan/poly(vinyl alcohol) clay nanocomposites. Mater Sci Eng C. 2015;56:363–73. doi: 10.1016/j.msec.2015.06.043.
[50] Chandran S, Sunny JC, Chandran S, Bellan C. Enhanced antimicrobial activity of *Aloe vera* blended zinc oxide nanoparticles in PVA matrix. Mater Today-Proc. 2018;5(8):16190–8. doi: 10.1016/j.matpr.2018.05.108.
[51] Ramesh M, Anbuvannan M, Viruthagiri G. Green synthesis of ZnO nanoparticles using *Solanum nigrum* leaf extract and their antibacterial activity. Spectrochim Acta A. 2015;136:864–70. doi: 10.1016/j.saa.2014.09.105.
[52] Das SK, Das AR, Guha AK. Gold nanoparticles: Microbial synthesis and application in water hygiene management. Langmuir. 2009;25(14):8192–9. doi: 10.1021/la900585p.

# Appendix

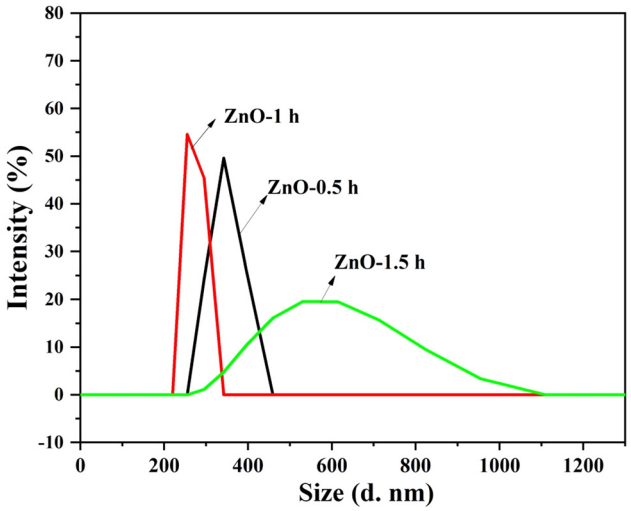


**Figure A1:** Particle size distribution of ZnO from dynamic light scattering (DLS) analysis.

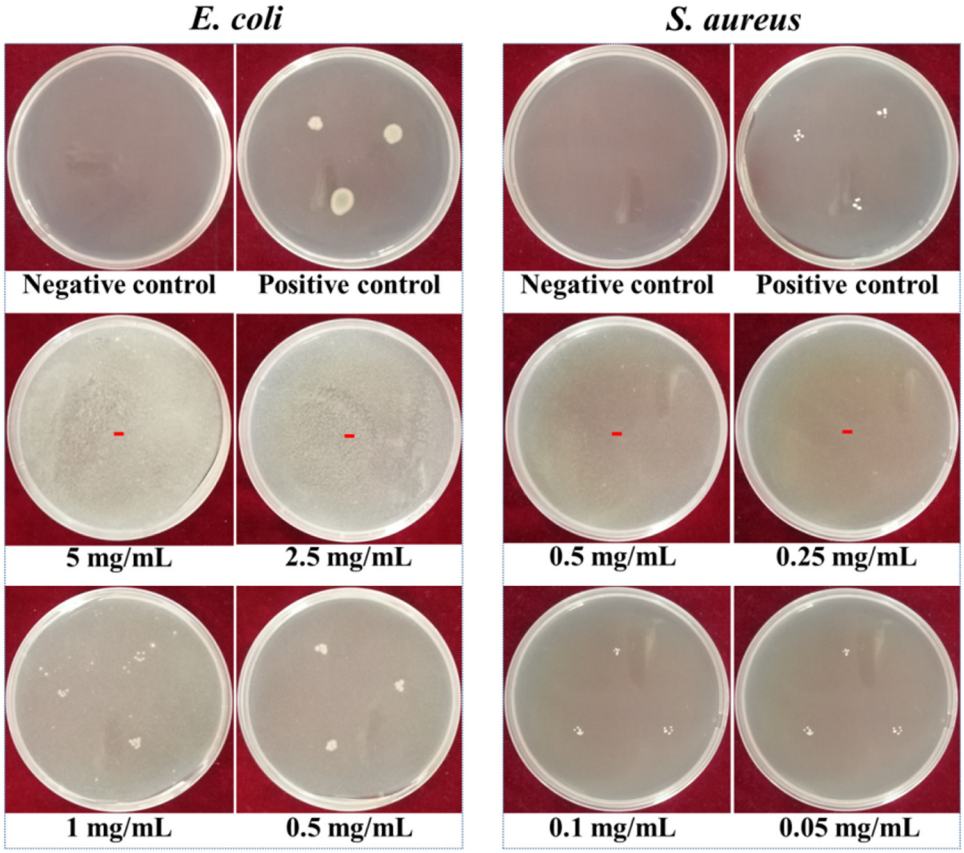


**Figure A2:** MIC values of pure ZnO against *E. coli* and *S. aureus*.

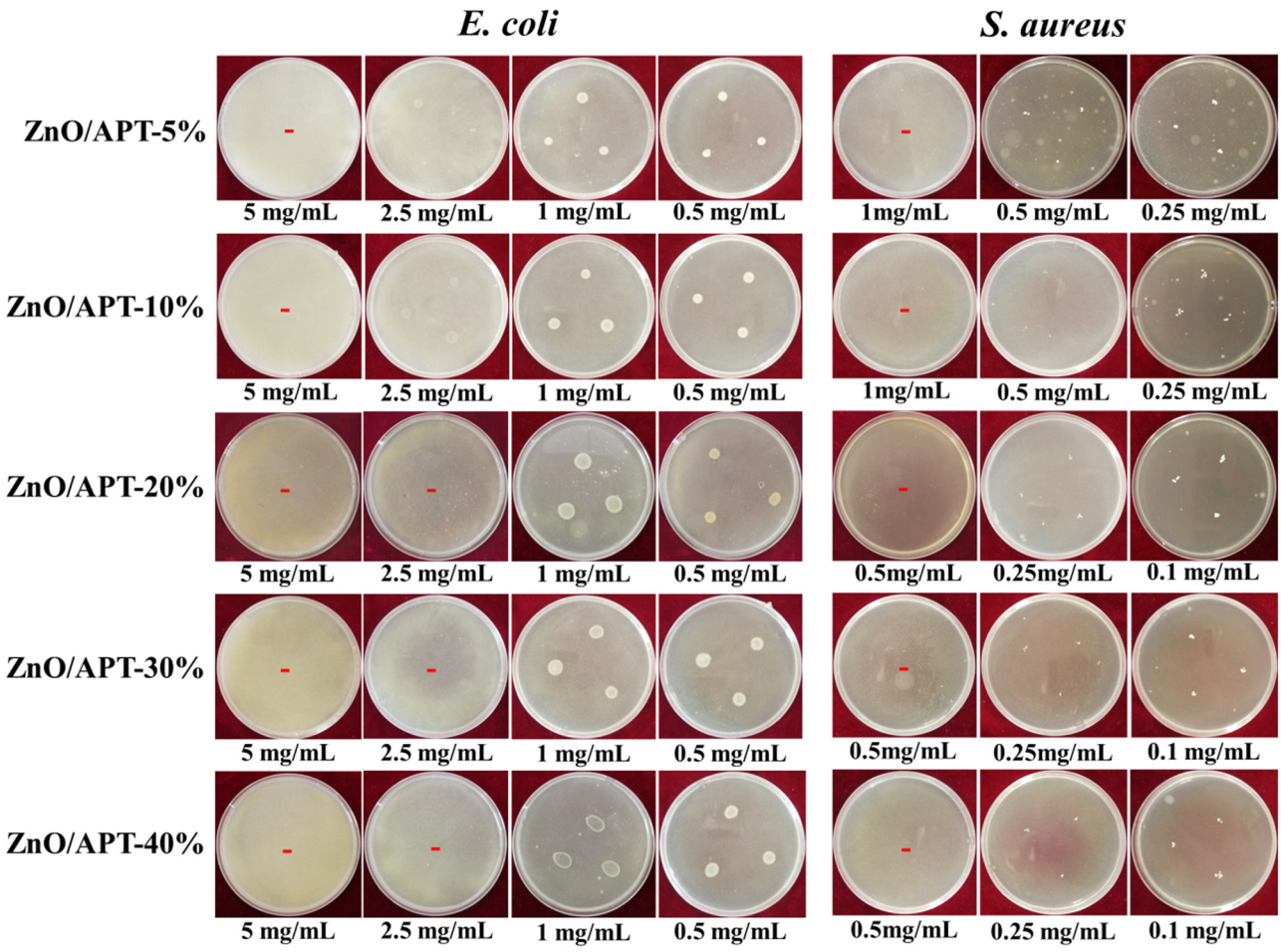


**Figure A3:** MIC values of ZnO/APT nanocomposites against *E. coli* and *S. aureus*.